Available online at www.sciencedirect.com
SCIENCE DIRECT®
Journal of Electrostatics 64 (2006) 604–610
Journal of ELECTROSTATICS
www.elsevier.com/locate/elstat

Steady control of laminar separation over airfoils with plasma sheet actuators

Roberto Sosa[a], Guillermo Artana[b,*]

[a]Laboratorio de Fluidodinámica, Facultad de Ingeniería, Universidad de Buenos Aires, Paseo Colón 850, C1063ACV, Buenos Aires, Argentina
[b]Laboratorio de Fluidodinámica, Facultad de Ingeniería, Universidad de Buenos Aires, CONICET, Paseo Colón 850, C1063ACV, Buenos Aires, Argentina

Available online 14 November 2005

Abstract

This work analyzes the effects produced by an EHD actuator on the flow around an airfoil at low *Re* numbers ($Re \approx 10^4$). The analysis is undertaken from flow visualizations and measurements of the surface pressure distributions. The experiments indicate that, for low *Re* number, the effects of the actuation depend on the power added to the flow and on the relative distance between the actuator and the separation line.

Keywords: Airfoil; Flow control; Laminar separation; EHD; Plasma

1. Introduction

The performance of airfoils operating at low *Re* number, has been providing increasing interest as a result of the desire to improve the performance of general aviation aircraft at low-speed, high-aspect-radio sailplanes wings, as well as to improve the design of remotely piloted vehicles, jet engine fan blades, and propellers at high altitude. The inboard sections of helicopter rotors, wind turbine rotors, and free-flying model aircraft also represent applications where low Reynolds number performance is important.

Different significant problems may contribute to diminish the aerodynamic performance of the airfoils with cord Reynolds number lower than about 200.000. Flow control in this area has focused on the mitigation of these problems, using different strategies like flapping or flexible wings [1] or boundary layer control (e.g., blowing, suction, etc.) [2–4].

The use of electrohydrodynamic (EHD) actuators was proposed some years ago. These actuators produce ionization of the flowing air and add localized momentum to the flow through a collision process of the migrating charged particles with the neutral species of the gas. EHD phenomena are based on the fact that currents involved are so low that the intensities of the magnetic forces are negligible compared to the electric ones. The main advantages of the EHD actuators are that they have no moving part, a very short response time (delays in the establishment of a discharge are theoretically of the order of nanoseconds) and a relatively good efficiency in transforming electrical to mechanical energy [5].

EHD actuators may be divided into three large groups: corona-based devices [6,7], dielectric barrier discharge devices [8,9] and plasma sheet devices [5,10,11].

Plasma sheet devices use generally two air-exposed electrodes flush mounted on the surface of a dielectric body separated by a few centimeters. The electrodes may be excited with a continuous (DC) or with a periodic potential difference. The device produces a homogeneous luminescence that occupies the interelectrode space along the span. In this region, the surface is covered by a thin film of ionized air. In some cases, a third electrode may be added to the system to ameliorate the stability of the discharge [12].

The objective in this work is to study the improvement of the aerodynamic performance of an airfoil operating at low Reynolds number ($Re < 50.000$) by means of a plasma sheet device working with a DC potential difference.

*Corresponding author. Tel: +54 (11) 4343 0891/4343 2775x383.
E-mail address: gartana@fi.uba.ar (G. Artana).

0304-3886/$ - see front matter © 2006 Elsevier B.V. All rights reserved.
doi:10.1016/j.elstat.2005.10.029

2. Experimental setup

2.1. Wind tunnel and airfoil

Flow visualization was utilized in an open low-speed wind tunnel (velocity ranges 0–5 m/s-rectangular cross-section of $0.45 \times 0.45\,m^2$) with a turbulence level of the air flow below 3%.

The airfoil shape was a NACA 0015 cross-section fabricated from polymethyl metacrylate (PMMA) with a cord dimension $c = 200$ mm and a spanwise dimension $b = 450$ mm. The airfoil was fabricated in two separate parts (male and female) matched to obtain a hollow body. The airfoil was suspended on both ends using pieces of electrical insulating material (nylon).

2.2. Flow visualization

The flow visualization at low-speed air velocities (≈ 1 m/s) were utilized using a paraffin oil smoke generator. This device allowed the creation of a single smoke filament that had an approximate diameter of $\phi_f = 2.5$ mm. A laser sheet intercepted the smoke filament assisting the visualization. The laser sheet had an approximate thickness of 0.5 mm and was generated by a 5 mW diode laser mounted on the ceiling of the probe section. The flow visualization was recorded with a digital video camera.

2.3. Pressure measurements

The pressure along the airfoil surface (P_i) was measured by means of 30 pressure ports that were drilled at the half of the span location of the airfoil. The tapped hole diameter was 1.5 mm and electrical insulating tubes of Tygon ($\phi_{int} = 0.5$ mm) were inserted in the holes, passed through the hollow of the airfoil and brought out through one end support of the model.

The static pressure of the free stream (P_0) was sensed using a tab mounted on the ceiling of the test section upstream the model. An electronic micromanometer was used to determine the differential pressure (P_i–P_0), in the pressure range between 0 and 0.1 WC inches (0–24.9 Pa) with accuracy of 1.0%. The electrical signals of the transductor at each tab were recorded using a data acquisition system.

For the present study the pressure coefficient C_p is defined as

$$C_p = \frac{P_i - P_0}{0.5\rho U_0^2} \tag{1}$$

where P_i is the surface pressure at station i, ρ the gas density, and U_0 the freestream velocity.

In regions where the flow was separated, the surface pressure at the different ports was unsteady and the value of the pressure considered there was a time-averaged value obtained by the direct measurement of the fluctuating surface pressure integrated over the time T of the experiment [11].

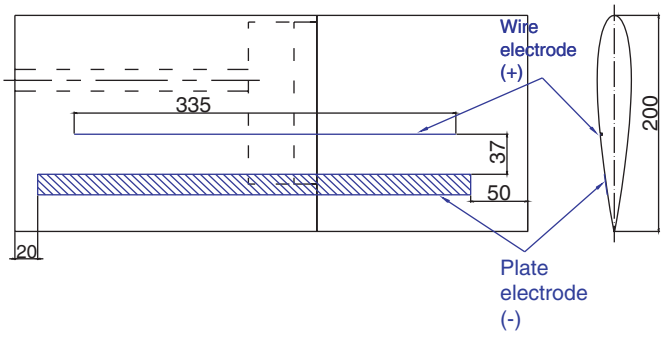

Fig. 1. Electrodes location on the airfoil surface (distances are in mm).

2.4. The coefficients of lift and of drag pressure

The coefficient of lift, $C_l(\alpha)$, and drag pressure, $C_{Dp}(\alpha)$, were calculated by integrating the distribution of the value of the coefficient C_p around the airfoil.

The $C_l(\alpha)$ and $C_{Dp}(\alpha)$ have been, in consequence, time-averaged values that hid the dynamic behavior of the lift and drag forces. However, they could give a fruitful data and result in a useful tool to compare the aerodynamic performance of the airfoil in the presence or in absence of the discharge.

2.5. Velocity measurement

Velocity measurements of the flow (U_0) were taken with a micromanometer (accuracy 0.04 Pa) and a Pitot probe located 0.15 m upstream the airfoil leading edge.

2.6. EHD excitation

Two different DC H.V. sources of opposite polarity (+20 kV, −20 kV, 1.5 mA) were used to apply the voltage differences between the two electrodes. The electrodes were located flush mounted on the suction surface of the airfoil.

A copper wire of 0.9 mm diameter was fitted in a slot of the airfoil surface at $x/c = 0.55$. The plate electrode consisted of a strip of 3.5 mm width of thin aluminum foil (50 μm thick) located at $x/c = 0.79$ (Fig. 1).

The wire electrode was connected to the source with a positive polarity while the plate electrode was attached to the negative polarity.

3. Experimental results

The range of velocities and angles of attack tested in our sets of experiments includes those associated with the occurrence of different phenomena [13]:

- flows with laminar boundary layer almost fully attached to the surface of the model,

- flows with laminar boundary layer separation: partially or fully separated
- flows with laminar separation bubbles (with or without downstream separation of the reattached turbulent boundary layer)

The effects of a discharge on the airflow depend on the characteristics of the regime considered.

3.1. Flow visualization and surface pressure distribution

The results of the flow visualization experiments and of the mean pressure distribution on the airfoil surface are presented in this section. For a better interpretation of the tests, the dimensionless pressure distribution (C_p vs. x/c) are accompanied by the solutions of a theoretical potential flow [14] and of a theoretical viscous flow (obtained from the XFOIL 1.0 program written by M. Drela [15]).

3.1.1. Laminar boundary layer almost fully attached

In the low range of Reynolds numbers (below 30.000), the flow conditions are normally such that the boundary layer is still laminar downstream the point (line) at which the pressure recovery on the airfoil surface commences and, provided the pressure gradient is moderate, a complete laminar flow can occur for small angles of attack [16].

When the airfoil is disposed at a zero angle of attack ($\alpha = 0^\circ$), a laminar separation position close to the trailing edge may be expected [17]. Typical results of the dimensionless pressure distributions considering this angle are shown in Fig. 2. The upper surface (extrados) pressure shows a pressure plateau near the airfoil trailing edge (theoretically starting at $x/c \approx 0.65$). This pressure plateau indicates the flow separation in this region.

As can be seen in the same figures, the effect of the discharge resulted in a modification of this plateau. In the last port, a continuous suction towards the trailing edge can be observed which indicates that separation was eliminated when the EHD actuation was activated.

On the lower surface of the airfoil (intrados), the actuation increased the value of the pressure in all ports. These results indicate a decrease of the velocity in this region of the flow.

With no discharge, the flow was separated, and in correspondence with the wake, there existed an important deficit of mass flow. To satisfy the mass conservation, the flow compensated this deficit by an increase in velocity in other regions of the section.

When the discharge was activated, the flow became fully (or partially) reattached, the wake disappeared (or diminished its wideness), and the regions of irrotational flow no longer needed to compensate the deficit of mass flow. In consequence, the observed decrease of the velocity on the lower surface of the actuated flow corroborates that the EHD actuation eliminated separation

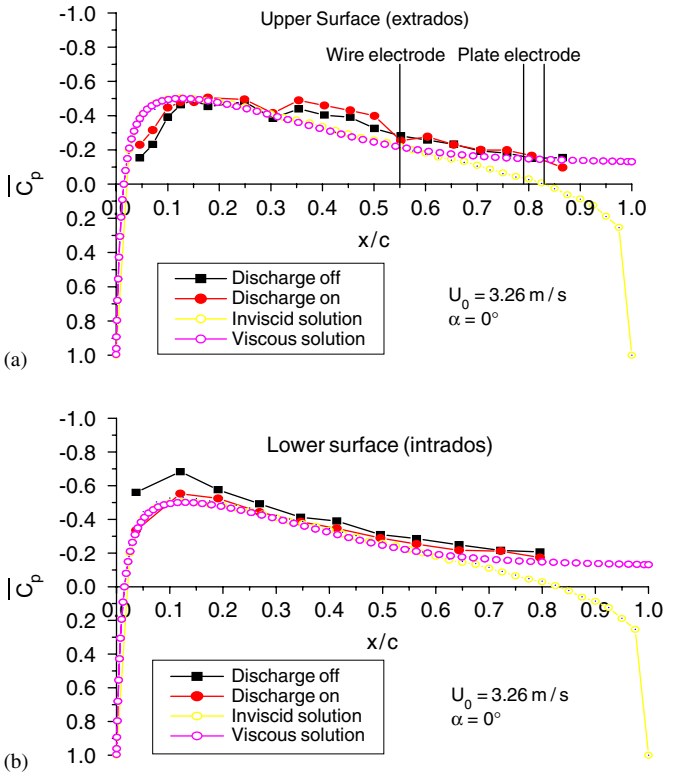

Fig. 2. Dimensionless pressure distribution ($Re = 43.466$, $\alpha = 0^\circ$, $\Delta V = 30\,\text{kV}$, $I = 250\,\mu\text{A}$). Upstream electrode positive. (a) (top) Upper surface, (b) (bottom) lower surface.

3.1.2. Laminar boundary layer separation

When increasing the angle of attack of the airfoil, the laminar separation point changes its position and different flow configurations with boundary layers partially or fully separated may take place.

Fig. 3 is a typical flow visualization of the partially separated flow configuration obtained with $\alpha = 5.3^\circ$ and $U_0 = 1\,\text{m/s}$.

The flow separation with actuation off (Fig. 3a) was revealed by the smoke filament that did not duplicate the shape of the airfoil surface and by the deformation of the smoke filament downstream the trailing edge. This deformation was attributed to the phenomenon of vortex shedding that induced an oscillatory movement of the smoke filament.

From this figure, the location of the separation point (line) may be roughly estimated, considering that downstream this point the distance between the smoke filament and the airfoil surface continuously increases. Taking into consideration this procedure in this experiment, the laminar separation point with no actuation was estimated at $x/c \approx 0.3$.

When the electric discharge was applied (Fig. 3b), the smoke filament gently contoured the airfoil surface. Note that even in the region of the trailing edge (circled region), the flow remained attached.

These results suggest that the EHD actuator eliminated the boundary layer separation. However, it should be

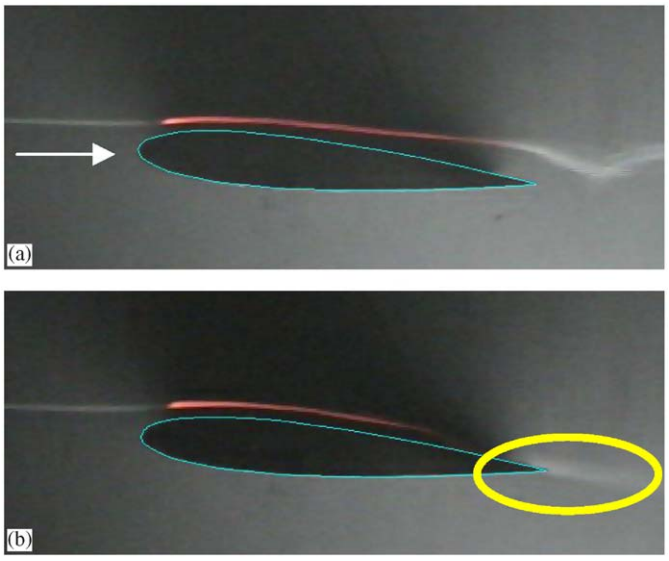

Fig. 3. Flow visualization ($Re = 15.000$, $\alpha = 5.8°$, $\Delta V = 30\,\text{kV}$, $I = 250\,\mu\text{A}$). Upstream electrode positive. (a) (top) Discharge off, (b) (bottom) discharge on.

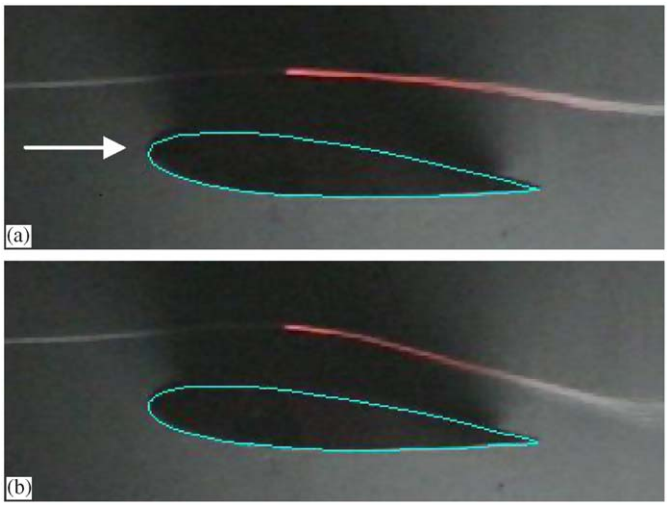

Fig. 4. Flow visualization ($Re = 15.000$, $\alpha = 5.8°$, $\Delta V = 30\,\text{kV}$, $I = 250\,\mu\text{A}$). Upstream electrode positive. (a) (top) Discharge off, (b) (bottom) discharge on.

noticed that the trajectories of the tracers may not agree with those of the neutral fluid particles and careful analyses of the filament visualizations have to be undertaken to avoid misinterpretation of the experimental results. A contamination of experimental results may occur in some tests when the smoke particles flowing at the vicinity of the electrodes attain an electric charge by ion impact. These spurious tracers may experience coulombian forces that are absent on the electrically neutral fluid particles and, in consequence, are no longer useful to track the fluid particles.

For this reason, visualizations were also undertaken with the smoke filament placed quite far away from the airfoil surface. (Fig. 4).

With discharge off (Fig. 4a), the filament corroborated the flow separation from the airfoil surface. When the discharge was established (Fig. 4b), again the filament copied the airfoil shape and an almost constant distance from the filament to the airfoil surface could be observed.

An analysis of the pressure distribution on the airfoil surface shows that with actuation off, the experimental results agreed well with the viscous flow solution (Fig. 5) and on the extrados, the pressure was almost constant at positions downstream the coordinate $x/c \approx 0.3$. The flow visualization experiments (Fig. 3a) without discharge also indicated that the separation of the boundary layer corresponded to this coordinate.

The actuation of the flow produced large alterations on the pressure distributions, and when the discharge was applied, it almost agreed with the potential (or inviscid) flow solution. On the extrados surface, larger suctions were observed and the plateau existing there without actuation disappeared under the action of the discharge. As in the flow visualization experiments, such behavior indicated the

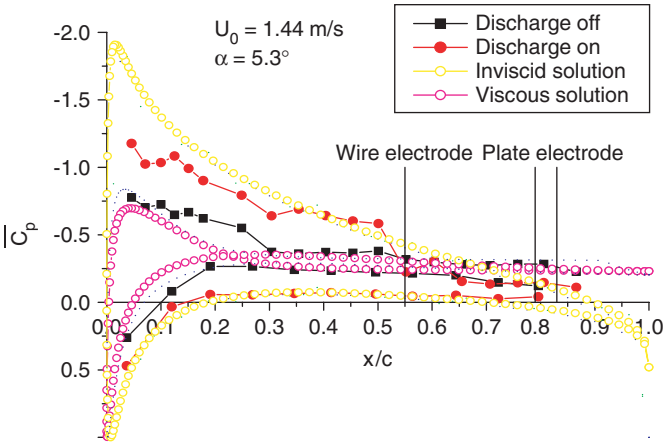

Fig. 5. Dimensionless pressure distribution ($Re = 19.200$, $\alpha = 5.3°$, $\Delta V = 30\,\text{kV}$, $I = 250\,\mu\text{A}$). Upstream electrode positive.

absence of laminar flow separation. On the airfoil intrados, the discharge also produced important pressure increases. These pressure increases may be associated to a flow deceleration in this region and were consistent with the flow reattachment observed in the upper surface.

Based on these results, we consider that the actuator produced a complete elimination of the laminar flow separation.

3.1.3. *Fully separated laminar boundary layer*

In this paragraph, we analyze a set of flow conditions that lead to a separation of the boundary layer quite close to the leading edge.

Fig. 6 shows the flow visualization for $\alpha = 5.3°$ and $U_0 = 1\,\text{m/s}$ at two different positions in height of the smoke filament.

With actuation off (Fig. 6a), the continuous increase of the distance of the smoke filament to the airfoil surface was

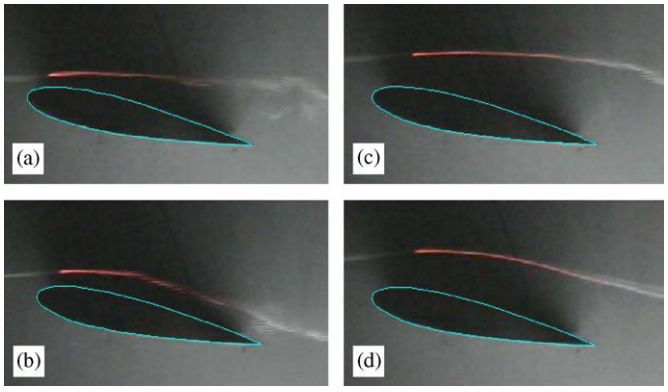

Fig. 6. Flow visualization with two different heights for the smoke filament ($Re = 15.000$, $\alpha = 11.7°$, $\Delta V = 30\,\text{kV}$, $I = 250\,\mu\text{A}$). Upstream electrode positive. Height 1: (a) discharge off and (b) discharge on. Height 2: (c) discharge off and (d) discharge on.

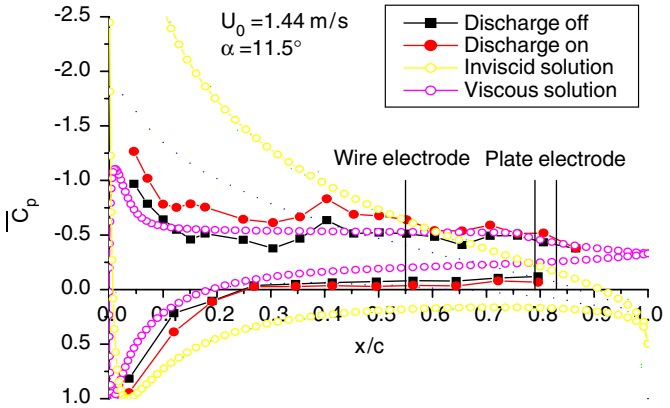

Fig. 7. Dimensionless pressure distribution ($Re = 19.200$, $\alpha = 11.5°$, $\Delta V = 30\,\text{kV}$, $I = 250\,\mu\text{A}$). Upstream electrode positive.

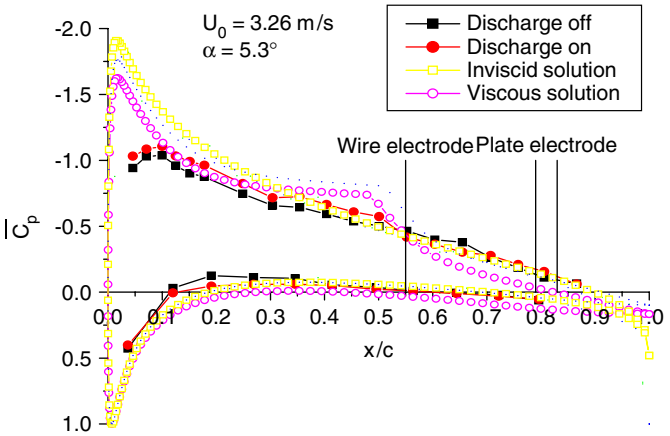

Fig. 8. Dimensionless pressure distribution ($Re = 43.466$, $\alpha = 5.3°$, $\Delta V = 30\,\text{kV}$, $I = 250\,\mu\text{A}$). Upstream electrode positive.

a sign of the boundary layer separation. Based on this figure, we could roughly estimate, as in the former case, that the separation point (line) occurred at $x/c \approx 0.1$.

During the application of the electric discharge (Fig. 6b), the smoke filament showed an unsteady behavior. The flow configuration oscillated from the one observed in Fig. 6a to the one in Fig. 6b where separation almost seems absent.

For Figs. 6c and d the smoke filament was again placed far from the airfoil surface in order to neglect the effect of spurious-charged tracers. When the discharge was not applied (Fig. 6c), the filaments almost did not curve around the body. The actuation enabled a better contouring of the flow around the airfoil (Fig. 6d), but again in this test the oscillating behavior was repeated.

From the extrados pressure distributions (Fig. 7), it is possible to estimate the position of the boundary layer detachment. In this case, discharge off the characteristic plateau of a separated flow indicated that separation occurred close to $x/c \approx 0.15$. These results agreed well with the flow visualization experiments (Fig. 6c).

The actuator activation produced larger suctions on the extrados and a slight recovery of pressure at positions $x/c > 0.4$. On the other hand, on the intrados of the airfoil, the actuator induced a flow deceleration, which indicates the slight overpressures registered there.

Based on these results, we consider that the actuator produced only a partial or intermitent elimination of the fully separated laminar boundary layer.

3.1.4. Laminar separation bubble

When a laminar boundary layer separates from the airfoil surface, the separated shear layer very rapidly undergoes transition to a turbulent flow. At a certain critical value of the Reynolds number, the turbulent mixing and entrainment processes make it possible for the flow to reattach to the surface as a turbulent boundary layer (TBL). This flow configuration is usually called laminar separation bubble (LSB).

The bubble position and size depend on the airfoil characteristics, on the Reynolds number and on the angle of attack [17]. Downstream the LSB, the reattached turbulent boundary layer may also suffer again a separation from the airfoil surface (separated TBL).

3.1.5. LSB without separation of the reattached turbulent boundary layer

We analyze a flow condition ($\alpha = 5.3°$ and $U_0 = 3.26\,\text{m/s}$) where the viscous flow solution predicts a LSB without further downstream separation.

The bubble extends approximately from $x/c \approx 0.1$ to 0.5 and the reattachment position of the LSB (Fig. 8) is determined in concordance with the position of a discontinuity in the slope of the pressure distributions on the extrados surface.

Fig. 8 enables one to observe that the pressure distributions of the experiments without actuation corresponded approximately with the viscous solution. However, the bubble size seemed larger with a reattachment at a

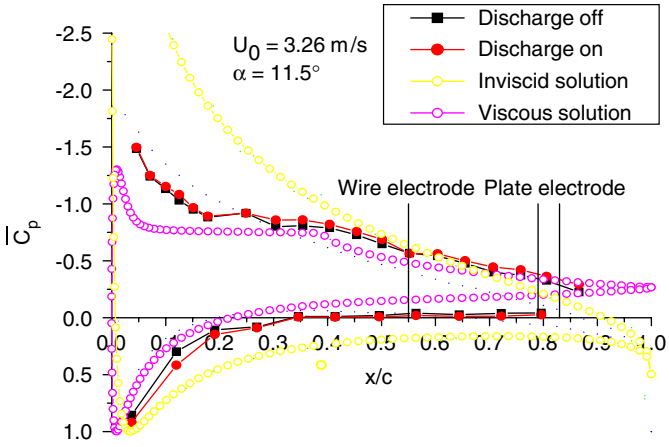

Fig. 9. Dimensionless pressure distribution ($Re = 43.466$, $\alpha = 11.5°$, $\Delta V = 30\,\text{kV}$, $I = 250\,\mu\text{A}$). Upstream electrode positive.

position ($x/c \approx 0.65$) downstream the one predicted by the viscous model.

The discharge application produced flow accelerations along the extrados in positions upstream the actuator. The reattachment of the LSB occurred at $x/c \approx 0.50$ and on the intrados only slight flow decelerations were observed.

As a result of the actuation the bubble size and position seemed to experience only slight changes.

3.1.6. LSB with separation of the reattached turbulent boundary layer

Fig. 9 shows the dimensionless pressure distribution, when $\alpha = 11.5°$ and $U_0 = 3.26\,\text{m/s}$. With this flow conditions, the viscous model estimates that the LSB is very short and the reattached turbulent boundary layer almost separates from the leading edge ($x/c = 0.05$).

With actuation off, the pressure distributions on the airfoil surface were in agreement with the viscous model.

The discharge activation produced very slight flow acceleration on the extrados of the airfoil at positions downstream $x/c \approx 0.3$ but no clear flow reattachment could be observed. In harmony with this behavior the flow deceleration on the intrados was almost negligible.

4. Conclusions

In previous sections, it has been shown that the effects of the actuator depend on the flow conditions (angles of attack and flow velocities). A good synthesis of these results can be obtained if we analyze the lift and drag pressure coefficients as a function of α, U_0 and the intensity level of the actuation.

The intensity of the actuation is here evaluated with a non-dimensional power coefficient C_W defined as

$$C_W = \frac{W}{0.5\rho U_0^3 b\delta}\left(\frac{L_{ele}}{c}\right)^2, \qquad (2)$$

Table 1
Aerodynamic coefficients as a function of flow conditions and actuation intensity

Flow condition	α (°)	Re (10^{-4})	Boundary layer flow on actuator/separation position	C_w (10^{-3})	Actuation effect	$C_{l(on)}$	ΔC	$C_l/C_{Dp(on)}$	$\Delta(C_l/C_{Dp})$
1	0.0	4.4	Separated LBL ($x/c = 0.65$)	0.16	Reattachment	0.02	0.05	−1.48	0.17
2	5.3	1.9	Separated LBL ($x/c = 0.35$)	1.80	Reattachment	0.41	0.21	16.72	5.82
3	11.5	1.9	Separated LBL ($x/c = 0.10$)	1.80	Intermittent reattachment	0.56	0.15	3.73	0.23
4	5.3	4.4	Attached TBL (upstream large LBS) ($x/c = 1$)	0.16	Slight Reduction of the bubble size	0.47	0.03	16.28	−1.02
5	11.5	4.4	Separated TBL (upstream short LBS) ($x/c = 0.15$)	0.16	Slight acceleration of the separated flow	0.65	0.03	4.26	−0.24

$C_{l(on)}$: lift coefficient with actuation on. $C_l/C_{Dp(on)}$: ratio of the lift coefficient to the drag pressure coefficient with actuation on. ΔC_l: difference on lift coefficient (actuation on minus actuation off). $\Delta(C_l/C_{Dp})$: difference on the C_l/C_{Dp} ratios (actuation on minus actuation off).

where L_{ele} is the inter-electrode distance, b the electrode length, δ the thickness of the plasma sheet and c the airfoil cord. The parameter W is the power of the discharge and may be easily calculated as the product of the discharge current I and the applied voltage difference between electrodes ΔV.

The same power coefficient in terms of other usual dimensionless parameter [18] can be expressed as

$$C_W = \frac{E_{HD}}{Re^2}\frac{v_i}{U_0}\left(\frac{L_{ele}}{c}\right)^2, \quad (3)$$

where: $Re = U_0 c/\vartheta$; $E_{HD} = Ic^3/A\rho\vartheta^2\mu_i$ and $A = b\delta$ the discharge section, ρ and v respectively the density and kinematic viscosity of the fluid, and μ_i the mobility of ions. The ions velocity v_i of Eq. (3) can be estimated with: $\mu_i E_0 \approx \mu_i(\Delta V/L_{ele})$.

Table 1 shows the effect of the discharge on the aerodynamic coefficients at the different flow conditions of our study.

The actuation of flows with LBL separation produced the full reattachment of the flow in the first two conditions, a lower value of C_W being required to produce the complete flow reattachment for the first case.

In the flow condition 3 for the same intensity level of the actuation (same values of C_W) of the flow condition 2, the increase on aerodynamic coefficients proved much less important.

On the other hand, taking into account different flow regimes but similar flow separation positions (flow conditions 3 and 5), the increase of lift coefficient and improvement of the ratio C_l/C_{Dp} has been more significant when a higher C_W coefficient was employed.

The fourth flow configuration corresponds to a large LSB without downstream flow separation. In this condition the discharge acts on a region where the boundary layer is turbulent and attached to the airfoil surface. The effects on the aerodynamics coefficients were quite reduced with a slight increase in C_l coefficient and a small degradation of the C_l/C_{Dp} ratio.

These results enable to highlight that the efficiency of actuation depend, among other parameters, on the distance between the position of the actuator and the laminar separation point (line). As a result, the following conclusions are proposed:

- the relative distance between actuator and separation line reveals a crucial parameter for low aerodynamics flow control,
- the higher this distance the higher the intensity level required to achieve similar effects,
- the actuation on flows with LSB in regions where the flow is attached is less effective.

Acknowledgments

This research has been done with grants UBACYT I024 and PICT 12-09482 of the Argentine government.

References

[1] W. Shyy, M. Berg, D. Ljungqvist, Flapping and flexible wings for biological and micro air vehicles, Prog. Aerosp. Sci. 35 (1999) 455–505.
[2] K.B.M.Q. Zaman, D.J. McKinzie, Control of laminar separation over airfoils by acoustic excitation, AIAA J. 29 (7) (1991) 1075–1083.
[3] A. Seifert, T. Bachar, I. Wygnanski, Application of active separation control to a small unmanned air vehicle, J. Aircraft 36 (2) (1998) 474–477.
[4] D. Greenblatt, I. Wygnanski, Use of periodic excitation to enhance airfoil performance at low Reynolds numbers, J. Aircraft 38 (1) (2000) 190–192.
[5] J. D'Adamo, G. Artana, E. Moreau, G. Touchard, Control of the airflow close to a flat plate with electrohydrodynamic actuators, ASME Paper No. 2002-31041, 2002.
[6] G. Colver, S. El-Khabiry, Modeling of DC corona discharge along an electrically conductive flat plate with gas flow, IEEE Trans. Ind. Appl. 35 (2) (1999) 387–394.
[7] C. Noger, J.S. Chang, G. Touchard, Active controls of electrohydrodynamically induced secondary flow in corona discharge reactor, in: Proceedings of the Second International Symposium on Plasma Technology in Pollution Control, Bahia, 1997, pp. 136–141.
[8] J.R. Roth, D. Sherman, Electrohydrodynamic flow control with a glow discharge surface plasma, AIAA J. 38 (7) (2000) 1166–1178.
[9] S.P. Wilkinson, Investigation of an oscillating surface plasma for turbulent drag reduction, AIAA Paper No. 2003-1023, 2003.
[10] G. Artana, R. Sosa, E. Moreau, G. Touchard, Control of the near wake flow around a circular cylinder with electrohydrodynamic actuators, Exp. Fluids 36 (6) (2003) 580–588.
[11] R. Sosa, E. Moreau, G. Touchard, G. Artana, Stall control of airfoils at high angle of attack with periodically excited EHD actuators, AIAA Paper No. 2004-2738, 2004.
[12] C. Louste, G. Artana, E. Moreau, G. Touchard, Sliding discharge in air at atmospheric pressure: electrical properties, J. Electrostat. 63 (2005) 615–620.
[13] R.F. Huang, C.L. Lin, Vortex shedding and shear-layer instability of wing at low-Reynolds numbers, AIAA J. 33 (8) (1995) 1398–1403.
[14] T. Theodersen, General potential theory of arbitrary wing sections, NACA Report #452, 1934.
[15] M. Drela, M.B. Giles, Viscous-inviscid analysis of transonic and low Reynolds number airfoils, AIAA J. 25 (10) (1987) 1347–1355.
[16] P.B.S. Lissaman, Low-Reynolds-number airfoils, Ann. Rev. Fluid Mech. 15 (1983) 223–239.
[17] T.J. Mueller, S.T. Batill, Experimental studies of separation on a two-dimensional airfoil at low Reynolds numbers, AIAA J. 20 (4) (1982) 457–463.
[18] IEEE-DEIS-EHD Technical Committee, IEEE Trans. DEI 10 (2003) 3–6.